



**HAL**  
open science

## Porogranular materials composed of elastic Helmholtz resonators for acoustic wave absorption

Stéphane Griffiths, Benoit Nennig, Stéphane Job

► **To cite this version:**

Stéphane Griffiths, Benoit Nennig, Stéphane Job. Porogranular materials composed of elastic Helmholtz resonators for acoustic wave absorption. *Journal of the Acoustical Society of America*, 2017, 141 (1), pp.254-264. 10.1121/1.4973691 . hal-01456305

**HAL Id: hal-01456305**

**<https://hal.science/hal-01456305>**

Submitted on 17 Feb 2017

**HAL** is a multi-disciplinary open access archive for the deposit and dissemination of scientific research documents, whether they are published or not. The documents may come from teaching and research institutions in France or abroad, or from public or private research centers.

L'archive ouverte pluridisciplinaire **HAL**, est destinée au dépôt et à la diffusion de documents scientifiques de niveau recherche, publiés ou non, émanant des établissements d'enseignement et de recherche français ou étrangers, des laboratoires publics ou privés.

# Porogranular materials composed of elastic Helmholtz resonators for acoustic wave absorption

Stéphane Griffiths, Benoit Nennig,<sup>a)</sup> and Stéphane Job

*Institut supérieur de mécanique de Paris (SUPMECA), Laboratoire Quartz EA 7393, 3 rue Fernand Hainaut, 93407 Saint-Ouen, France.*

(Originally published in JASA 141(1) <http://dx.doi.org/10.1121/1.4973691>)

We present a theoretical and experimental study of the acoustic absorption of granular porous media made of non-cohesive piles of spherical shells. These shells are either rigid or elastic, possibly drilled with a neck (Helmholtz resonators), and either porous or impervious. A description is given of acoustic propagation through these media using the effective medium models proposed by Johnson (rigid particles) and Boutin (rigid Helmholtz resonators), which we extend to the configurations studied in this work. A solution is given for the local equation of elasticity of a shell coupled to the viscous flow of air through the neck and the micropores. The models and our simulations are compared to absorption spectra measured in reflection in an impedance tube. The effective medium models and our measurements show excellent agreement for configurations made of rigid particles and rigid Helmholtz resonators that induce an additional peak of absorption at low frequency. A shift of the Helmholtz resonance toward low frequencies, due to the softness of the shells is revealed by our experiments for elastic shells made of soft elastomer and is well reproduced by our simulations. We show that microporous shells enhance and broaden acoustic absorption compared to stiff or elastic resonators.

PACS numbers: 43.55.+p, 47.56.+r, 43.20.Hq, 45.70.Cc

Keywords: Acoustic absorption; Porogranular medium; Double porosity; Shell elasticity; Helmholtz resonator

## I. INTRODUCTION

Granular materials are an interesting alternative to the standard porous materials generally used to absorb sound waves. Their ease of use and handling makes them ideal candidates for building applications, for instance. The physics of acoustic wave propagation in porous materials made of piles of non-cohesive particles has been widely studied over the last few years as an equivalent fluid<sup>1,2</sup> or via an extended Biot theory<sup>3</sup> to include the effect of contact dynamics between grains on the elastic response of a rigid frame. Practical applications such as the limitation of sound transmission through double leaf panels filled with polystyrene beads has been investigated by Chazot and Guyader<sup>4,5</sup>. Regarding sound absorbing applications, Nennig et al.<sup>6</sup> improved the sound absorption of 2 millimeter glass beads by trapping modes in  $\sqcup$ -shape inclusions. These works showed the potential of such materials, regardless of their porosity.

Sound propagation in a porous medium with rigid Helmholtz resonators, for instance, rigid shells with a hole on their surface, has been investigated theoretically using periodic homogenization methods<sup>7,8</sup>, numerically<sup>9</sup> and experimentally<sup>8,9</sup>. In particular, Boutin et al.<sup>7,8</sup> provided the effective parameters for macroscopic wave propagation in such a metamaterial. In particular, he gave a detailed description of the effect of viscothermal dissipation in the pore network between the resonators and in the resonator necks. Although the losses are not

considerable, embedded Helmholtz resonators yield to an acoustic metamaterial with a negative bulk modulus and where group and phase velocities have an opposite sign, close to the resonator resonance. Similar results were observed by Fang et al. for a 1D array of resonators<sup>10</sup>. However, high viscothermal losses may limit resonator efficiency<sup>7,9</sup> if the matrix is in the viscous regime (near diffusion equation), *i.e.* when the frequency is above the viscous frequency (see appendix I). In our case, the viscous/inertial transition occurs at 44 Hz for the granular matrix.

Another interesting feature is the effect of the resonators elasticity on the global absorption of the granular medium, which introduces or affects resonant mechanisms and thus the peaks in the absorption spectrum. However, the effect of elasticity can be coupled with shell resonances to contribute another source of absorption to the system<sup>11</sup>. Up to now, very few works have focused on resonators with elastic shells. In the 1990s, Photiadis<sup>12</sup> and Norris et al.<sup>13</sup> investigated such materials for underwater acoustic applications. Norris et al. showed that the resonant frequency  $f_s = \sqrt{R_0}f_r$  of an elastic resonator can be shifted down in comparison to the resonant frequency  $f_r$  of a rigid resonator, by writing:

$$R_0 = \left( 1 + \frac{3}{2} \frac{r_m}{t} \frac{\gamma P_0}{E} (1 - \nu) \right)^{-1}, \quad (1)$$

which depends on the mean radius of the shell  $r_m$ , the shell thickness  $t$ , the Youngs modulus  $E$  and the Poisson's coefficient  $\nu$  of the shell material. The terms  $\gamma$  and  $P_0$  are the specific heat ratio and the atmospheric pressure, respectively. For airborne applications, with  $r_m/t \approx 10$ , the use of a material with a Youngs modulus of the order

---

<sup>a)</sup>Corresponding author; email : benoit.nennig@supmeca.fr

of 1 MPa or less leads to a significant shift  $f_s \approx 0.6f_r$ .

This work presents a comparison between experimental data and theoretical models relating to the sound absorption of poroelastic media made of rigid, elastic or microporous Helmholtz resonators with or without an extended neck. Here, the microporous character of the shell originates from the fabrication process of the naturally pervious elastomer. In our experiments, only airborne excitations were considered.

In the first part, after a brief reminder of the model of Boutin et al.<sup>7,8</sup> relating to rigid Helmholtz resonators, a lumped model is proposed as an extension to the configurations tested. In the second part, the different models are compared to absorption measurements and to results found in the literature.

## II. LUMPED PARAMETER RESONATOR MODELS

Here, we consider a granular medium composed of identical elastic resonators packed randomly to a given compaction (filling fraction)  $C = 1 - \phi$ , or porosity  $\phi$ , in view to finding the effective bulk modulus and density of the medium, excited by a harmonic airborne wave  $p^{\text{ext}}$  (time convention  $e^{-j\omega t}$ ), in the long wavelength approximation.

As shown by Boutin<sup>8</sup>, the flux of the resonator, obtained as the forced response to the macroscopic pressure wave, is one order of magnitude smaller than the flux between the grains of the porous matrix. Here, the *porous matrix*, denoted by the subscript  $m$ , stands for a virtual porous medium composed of the air contained between the impervious and rigid grains. This implies that the presence of the resonators does not change the global effective density (or permeability)  $\rho_{\text{eff}} = \rho_m$  of the medium or the bulk modulus  $E_m$  in the porous matrix (see appendix I). However, the effective bulk modulus of the granular medium,  $E_{\text{eff}}$ , is changed drastically according to

$$E_{\text{eff}} = \left( \frac{1-C}{E_m} + \frac{C}{E_r} \right)^{-1}, \quad (2)$$

where  $E_r$  is the effective modulus of the resonators. The aim of this part is to obtain a closed form estimation of the effective modulus of the resonators  $E_r$  in the long wavelength approximation. It is noteworthy that the following approach does not take into account the orientation and the possible interactions between the resonators<sup>14</sup>.

The model derived by Boutin et al.<sup>7,8</sup> can be extended by modifying the pulsed flux. The contribution of the elastic shell, or of its microporosity, can be added as supplementary fluxes coupled to the flux exiting the neck.

We consider a thin spherical elastic shell of thickness  $t$ , diameter  $d_s$ , area  $S_s$  and volume  $V_s$ , as shown in Fig. 1, made of an elastic material. As the particles are elastomer, they are incompressible. Its internal volume  $V_0$  is filled with a perfect fluid having a uniform pressure  $p$ . The shell has a cylindrical hole whose effect on the modal behavior of the shell is considered negligible. This neck

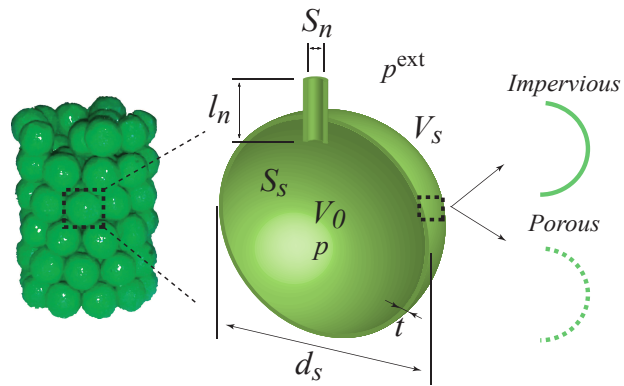


FIG. 1. Picture of the granular pack and sketch of a spherical resonator with its associated shell.

has a volume  $V_n$ , a length  $l_n$ , a section  $S_n$  and contains a mass  $m_n$  of fluid. Each micropore has a volume  $V_\mu$ , a length  $l_\mu$ , a section  $S_\mu$  and contains a mass  $m_\mu$  of fluid.

The acoustic radiation from a neck or micropore into the free space is taken into account via a correction length  $\delta_i = 8d_i/(3\pi)^{15}$  of  $l_n$  and  $l_\mu$ , with respect to their diameters  $d_i$  (with  $i = n, \mu$ ).

For small perturbations, and by neglecting losses, the fluid pressure in the cavity is defined by

$$p = -K_0 \nabla \cdot \mathbf{u}_a, \quad (3)$$

where  $K_0 = \gamma P_0 = \rho_0 c_0^2$  is the adiabatic bulk modulus of the fluid and  $\mathbf{u}_a$  is the acoustic displacement of the fluid. After integrating this equation in the volume of the cavity, the continuity of the acoustic displacement, assuming a uniform pressure field, yields

$$p = -\frac{K_0}{V_0} J \quad (4)$$

where  $J = \sum_i S_i u_i$  is the volumetric flux across the shell. Index  $i$  represents the shell ( $s$ ), the neck ( $n$ ) or the micropores ( $\mu$ ) of the shell. Here  $u_i$  and  $S_i$  stand for the radial displacement and the surface of these elements respectively.

The long wavelength approximation implies that  $p^{\text{ext}}$  is uniform around the shell. Assuming that the neck does not change the thin shell mode, the displacement  $u_s$  of the spherical shell can be assumed as purely radial and constant across the thickness. Thus the resonance frequency of the first breathing mode is given by Baker<sup>16</sup> and reads

$$\omega_s = \sqrt{\frac{2(1+\nu)E^*}{\rho_s r_s^2}}, \quad (5)$$

with  $\rho_s$  being the density of the material and  $r_s$  the radius of the shell. The term  $E^* = E/(1-\nu^2)$  depends on the elastic characteristics of the material and can be made complex to account for the viscoelastic losses. The lumped stiffness of the shell for the first radial mode (breathing mode) is thus defined as  $k_s = \omega_s^2 m_s$ , where

$m_s$  is the moving mass of the shell. Here, we do not consider the flexural modes<sup>11,16</sup> of the shell: they appear at lower frequency but do not imply a significant variation of volume.

In addition to the viscoelastic losses in the shell, dissipation occurs with capillary air flow in the neck and through the micropores. By considering the neck and the micropores as cylindrical channels, as shown in Fig. 2, the momentum equation can be reduced to the Eq. (4.9) of Ref. 17

$$-j\omega\rho_0\dot{u}_i(r) = -\frac{\partial p}{\partial n} + \frac{\eta}{r} \frac{\partial}{\partial r} \left( r \frac{\partial \dot{u}_i(r)}{\partial r} \right), \quad (6)$$

where  $\eta$  stands for the dynamic viscosity of air and  $\mathbf{n}$  for the outward normal vector of the shell.

The adherence boundary condition implies that  $\dot{u}_i(R_i) = \dot{u}_s$ , at  $r = R_i$ , with  $R_i$  being the radius of the channel ( $i = n, \mu$ ) and  $\dot{u}_s$  the mean velocity of the shell. After integration (see Eq. 4.9 in Ref. 17), this yields the total viscous force in a cylindrical pore of volume  $V_i = S_i l_i$

$$F_i(u_i, u_s) = V_i \rho_0 \omega^2 \frac{B_i}{1 - B_i} [u_i - u_s], \quad (7)$$

with  $B_i = \frac{2}{\beta R_i} \frac{J_1(\beta R_i)}{J_0(\beta R_i)}$ ,  $\beta = \sqrt{\frac{j\omega\rho_0}{\eta}}$  and where  $J_0$  and  $J_1$  stand for the Bessel function of the first kind. The viscous force depends on the relative difference between the mean velocity of air in the neck or in the micropores and the mean velocity of the shell.

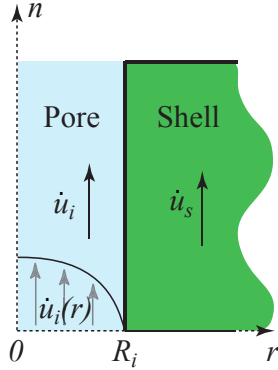


FIG. 2. Velocity profile in a micropore or in the neck.

We now focus on an impervious elastic shell having a neck. Using Eqs. (4), (5) and (7), the equations of motion of the lumped displacement of the shell and of the gas in the neck are

$$\begin{cases} -m_n \omega^2 u_n = -S_n \frac{K_0}{V_0} J + F_n(u_n, u_s) - p^{\text{ext}} S_n, \\ -m_s \omega^2 u_s = -k_s u_s - S_s \frac{K_0}{V_0} J - F_n(u_n, u_s) - p^{\text{ext}} S_s. \end{cases} \quad (8)$$

Here, the total flux reads  $J = S_n u_n + S_s u_s$ . The eigenvalue of the homogeneous problem ( $p^{\text{ext}} = 0$ ) without viscosity, allows estimating the different resonance modes

of the resonator. Moreover, the resolution of the system (8) for a constant harmonic external pressure  $p^{\text{ext}}$  makes it possible to compute the volumetric flux  $J$  and obtain effective bulk modulus of the resonators  $E_r$  in the long wavelength approximation

$$E_r(\omega) = V_0 \frac{p^{\text{ext}}}{J}. \quad (9)$$

The effective modulus  $E_{\text{eff}}$  of the granular medium is determined using Eq. (2). Knowing parameters  $E_{\text{eff}}$  and  $\rho_{\text{eff}}$  (see appendix I, Eq. (A2)) makes it possible to provide a full description of an effective medium.

When the neck is not present or in the case of a microporous shell, similar approaches are implemented, as presented in the next sections.

### III. EXPERIMENTAL RESULTS

The measurements are performed using an impedance sensor (provided by the Centre de Transfert de Technologie du Mans<sup>18</sup>, France) located at the top end of a tube having an internal diameter  $d_t = 22$  mm and a length  $l_t = 50$  mm (see Fig. 3a). The opposite side is closed by a rigid aluminum wall on which the sample of height  $h$  is placed. Impedance measurements are performed over the whole frequency range achievable by the sensor, from 20 Hz to 6000 Hz with sweep sine excitation.

Several configurations were tested, as summarized in Fig. 3. The shells themselves were either rigid (Fig. 3b) or elastic (Fig. 3c, d). In the latter case, the shells were porous or impervious. Three cases were measured for each type of shell: undrilled, simply drilled or drilled with an extended neck.

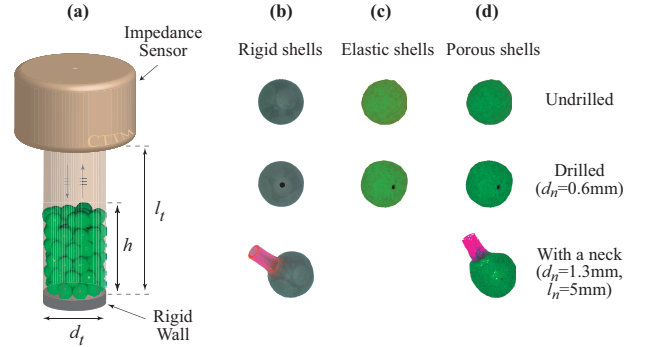


FIG. 3. (a) Sketch of the impedance tube and (b) rigid, (c) elastic and (d) porous shells used for the absorption measurements. The different configurations tested (undrilled, drilled or with a neck) are listed for each kind of shell.

In this setup, only plane waves propagate at normal incidence below 6000 Hz. The comparison with the model proposed is therefore straightforward. The acoustic reflection coefficient

$$R(\omega) = \frac{Z_{\text{layer}} - Z_{\text{air}}}{Z_{\text{layer}} + Z_{\text{air}}}, \quad (10)$$

is determined as a combination of the characteristic impedance of air  $Z_{\text{air}} = \rho_0 c_0$  and the complex surface impedance of the material  $Z_{\text{layer}} = jZ_{\text{eff}} \cot(k_{\text{eff}} h)$ , with  $Z_{\text{eff}} = \rho_{\text{eff}} c_{\text{eff}}$ , the characteristic impedance of the medium. The effective wavenumber  $k_{\text{eff}} = \omega/c_{\text{eff}}$  is related to the sound speed in the granular packing  $c_{\text{eff}} = \sqrt{E_{\text{eff}}/\rho_{\text{eff}}}$ . Then, the absorption coefficient is given by  $A(\omega) = 1 - |R(\omega)|^2$ .

The skeleton of the poroelastic material<sup>17,19</sup> can be considered as motionless above the decoupling frequency  $f_0 = \sigma\phi^2/(2\pi\rho)$  when subjected to fluid-born excitation if: i) the bulk moduli of the solid phase  $K_e$  and of the saturating fluid  $K_0$  are similar, and ii) the density of the solid phase  $\rho_s$  is higher than the density of the fluid  $\rho_0$ . Here, the density of the packed grains is  $\rho = (1 - \phi)\rho_p \approx 214 \text{ kg.m}^{-3} \gg \rho_0$ , where  $\rho_p = 384 \text{ kg.m}^{-3}$  is the density of one hollow spherical porous shell. The bulk modulus of the skeleton network of grains can be estimated from an effective medium theory that originates from Hertz-Mindlin interactions between particles<sup>20</sup>:  $K_e$  depends on the static load applied on the packing. In the first approximation, we estimate this load as the weight of the packing itself,  $F_0 \approx 9.10^{-4} \text{ N}$ . This gives<sup>20</sup>

$$K_e = \frac{k_n}{12\pi} (\phi Z)^{2/3} \left( \frac{6\pi p^{\text{stat}}}{k_n} \right)^{1/3} \quad (11)$$

where  $k_n = 4G/(1 - \nu)$  is the effective stiffness between two grains and  $G$  is their shear modulus. The term  $Z$  is the coordination number (set at  $Z = 6$  by assuming random close packing) and  $p^{\text{stat}}$  is the static pressure related to  $F_0$  and to the grain contact area. It turns out that the bulk modulus of the solid phase,  $K_e \approx 1.77.10^5 \text{ Pa}$ , has the same order of magnitude as the bulk modulus of air  $K_0 = 1.4.10^5 \text{ Pa}$ . Here, the decoupling frequency is equal to  $f_0 \approx 15.3.10^{-2} \text{ Hz}$ , meaning that the porous matrix can be considered as motionless over the whole frequency range of interest. The granular packing thus behaves like an equivalent fluid. Thus non-linear contact dynamics between particles is not involved, as confirmed by measurements performed at several excitation levels between 93 and 103 dB, showing no difference in frequency or in amplitude.

Various arrangements of particles were tested. Finally, despite a shift of the absorption peak due to the different height of each packing, no significant effect due to the granular arrangement was observed in the frequency range measured [20-6000] Hz (see Appendix II).

### A. Rigid shells

The rigid polymer shells (ref. P150603 provided by Ateca, France) used in this work had an external diameter of  $d_s = 5.55 \pm 0.15 \text{ mm}$  and a thickness of  $t = 0.34 \pm 0.06 \text{ mm}$  measured by microscope imaging analysis. Using a pycnometer the density of the shells was measured as  $\rho_s = 1488 \pm 84 \text{ kg.m}^{-3}$ .

The acoustic absorption was measured for different configurations of the shells, and is presented in Fig.4 and compared to the models. In every case, different heights of the packing were tested to experimentally identify the different absorption peaks corresponding to the quarter wavelength frequency  $f_{\lambda/4}$ , which scales as the inverse of the height of the sample, and to the Helmholtz frequency  $f_H$ , which depends solely on the characteristics of the resonators. The height and the compaction corresponding to the three configurations probed are summarized in table I. The quarter wavelength frequency

$$f_{\lambda/4} \approx \frac{1}{4h} \Re \left( \sqrt{\frac{\bar{E}_{\text{eff}}}{\bar{\rho}_{\text{eff}}}} \right), \quad (12)$$

is estimated by taking the mean values of the bulk modulus  $\bar{E}_{\text{eff}}$  and of the density  $\bar{\rho}_{\text{eff}}$  over the frequency band measured.

In the first case (Fig. 4a), the acoustic absorption is measured in a sample made of rigid and impervious shells (without holes). Here, the model reduces to the Johnson-Champoux-Allard (JCA) model<sup>17</sup> with the parameters given in appendix I. It can be observed that the JCA model agrees well with the measured data. The absorption corresponding to the quarter wavelength frequency is prominent and well described both in frequency and in amplitude by the JCA model.

A 0.6 mm diameter hole is then drilled in each shell; each particle now corresponds to a Helmholtz resonator whose neck length is equal to the thickness of the shell plus a length correction (see above). Our model reduces to :

$$-\omega^2 m_n u_n = -S_n \frac{K_0}{V_0} J - p^{\text{ext}} S_n + F_n(u_n, 0), \quad (13)$$

with  $J = S_n u_n$ . This model matches the model proposed by Boutin<sup>7,8</sup>.

As can be seen in Fig. 4b the models are indeed in good agreement. For both models, the length of the neck accounts for a length correction and the models are calculated using the same rigid frame porous parameters  $\rho_m$  and  $E_m$ . The only slight difference between the models stems from the way the dissipation is taken into account.

The models predict the quarter wavelength resonance at  $f_{\lambda/4} = 2080 \text{ Hz}$  quite well but they both fail to predict the Helmholtz resonance, found experimentally at  $f_H = 3980 \text{ Hz}$  and predicted theoretically 500 Hz lower. The difference between the experiments and the models is likely due to the high sensitivity of the system to the length correction, rendering the acoustic radiation at the holes. Indeed, the radiative reactance becomes the leading inertial term when the diameter of the aperture is larger than the thickness of the shells. However, the hole shape and its neighborhood on both sides can significantly modify the classical baffled circular piston end correction proposed by Ingard<sup>15</sup>. Next, the presence of a neck with a length greater than the end correction provides more reliable estimations, since the thickness becomes the leading inertial term and the system is less sensitive to uncertainty on the end correction.

In the third case, a tube with an inner diameter of 1.3 mm and length of 5 mm is placed in the hole, as shown in Fig. 1b. The models remain formally unchanged and good agreement between the experimental data and both models is observed in Fig. 4c. The model developed describes the quarter wavelength resonance at  $f_{\lambda/4} = 1770$  Hz and the Helmholtz resonance at  $f_H = 3000$  Hz well, both in frequency and amplitude. Even the last absorption peak corresponding to the  $3\lambda/4$  resonance is described well. The discrepancies between both models can be explained by the different ways the dissipation is taken into account in the estimation of the effective compressibility of the resonators  $E_r$ .

Configurations	Height $h$	$C$
Undrilled	$25.13 \pm 0.87$ mm	0.56
Drilled ( $d_n = 0.6$ mm, $l_n = t$ )	$25.30 \pm 1.43$ mm	0.56
Neck ( $d_n = 1.3$ mm, $l_n = 5$ mm)	$27.64 \pm 1.30$ mm	0.51

TABLE I. Heights and compactities corresponding to the 60 rigid shells used for absorption measurements.

## B. Elastic shells

The medium is now composed of elastic resonators made of elastomer (ref. E150403, provided by Ateca, France). The elastic shells have an external diameter  $d_s = 5.60 \pm 0.19$  mm and their thickness measured by SEM photographs is  $t = 0.33 \pm 0.04$  mm. The thickness and the external diameter are very similar to the rigid shells. The average mass of the particles is  $m_s = 36.7 \pm 1.4$  mg, and the density of the shells is measured using a pycnometer as  $\rho_s = 1202 \pm 23$  kg.m<sup>-3</sup>.

The Young's modulus of the material used to make the spheres is estimated as equal to  $E = 3(1 - 0.3j)$  MPa, which suits our experimental results well and is in line with the previous Dynamic Mechanical Analyzer (DMA) measurements for a 5 mm high and 18 mm diameter cylindrical sample of the same material, indicating a value of about 2 MPa. Although this is a fair estimation, the slight difference of elasticity can be attributable to the specifications of the elastomer curing process to fabricate a thin shell or a thicker bulk specimen instead. Since the elastomer is incompressible, the Poisson's ratio is set to  $\nu = 0.495$ .

The SEM photograph in Fig. 5a shows the presence of a small particle inside the elastomer shell, which is a polystyrene residue resulting from the fabrication process of the hollow elastomer shells. Its diameter is about 1 mm and is considered negligible as it represents only 0.88% of the internal volume.

The shells are naturally porous (Fig. 5b), thus a layer of acrylic coating was sprayed on their surface to make them impervious and to measure the absorption of non-porous elastic shells (Fig. 5c). Adding such a layer on the surface of the shells increases the elastic modulus  $E$ . It is inferred as equal to  $E = 4(1 - 0.3j)$  MPa.

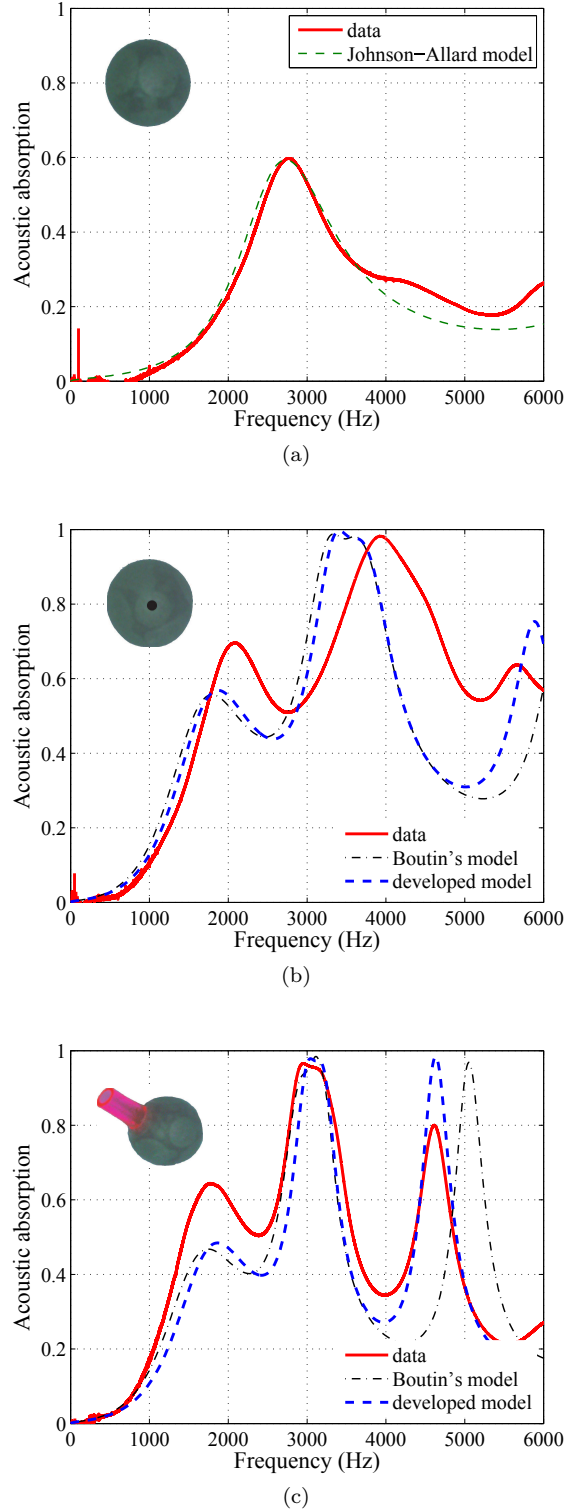
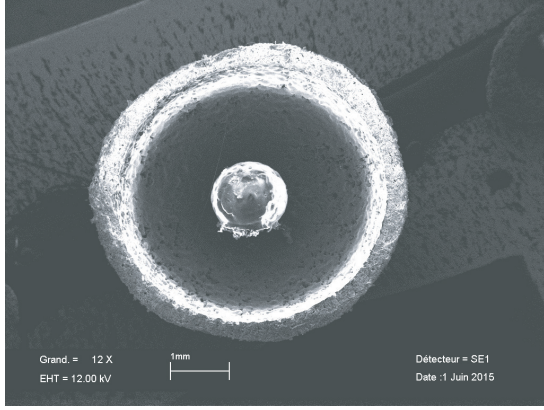
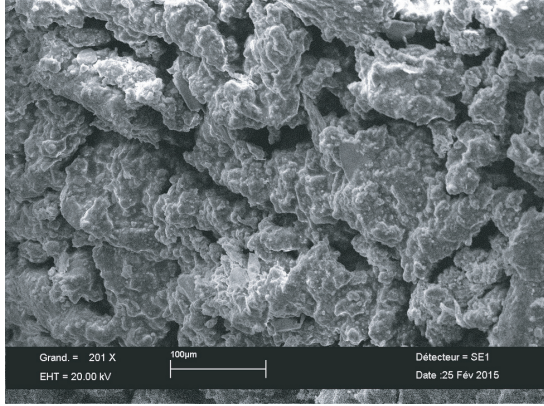


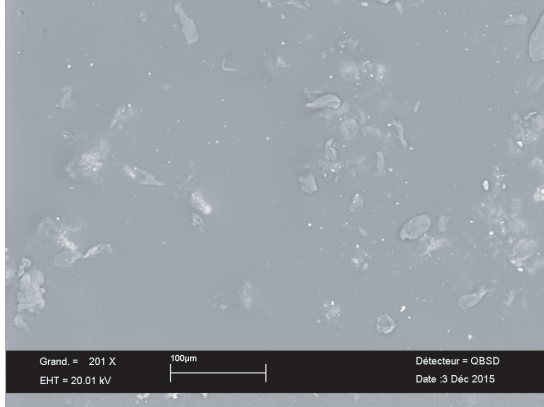
FIG. 4. Acoustic absorption measured for 60 rigid shells (—) compared to the model developed (---) and to the model given by Boutin (- · -) for (a) non drilled shells, (b) shells drilled with a 0.6 mm diameter hole and (c) shells 1.3 mm in diameter with a 5 mm long neck.



(a)



(b)



(c)

FIG. 5. (a) SEM photograph of an elastomeric resonator and (b) of its surface and (c) its surface after acrylic coating.

As with the rigid shells, the measurements were performed for non-drilled shells and for shells having a neck of 0.6 mm in diameter (see Fig. 3b). As previously, the samples contained 60 shells and Table II summarizes the heights and associated compactions.

For non-drilled shells, our model reduces to

$$-\omega^2 m_s u_s = -k_s u_s - S_s \frac{K_0}{V_0} J - p^{\text{ext}} S_s. \quad (14)$$

Configurations	Height $h$	$C$
Undrilled	$26.43 \pm 0.93$ mm	0.53
Drilled ( $d_n = 0.6$ mm, $l_n = t$ )	$25.18 \pm 0.73$ mm	0.55

TABLE II. Heights and compactities corresponding to the 60 elastic shells.

with  $J = S_s u_s$ . The comparison with measured absorption is presented in Fig. 6a. It shows that the model gives a good description of the absorption and the quarter wavelength peak is accurately modeled in both frequency and amplitude. When compared with the rigid shells (see Fig. 4a.) the elastic beads lead to a slight shift and widening of the quarter wavelength peak. The effect is small here because the shell is stiffer than the bulk modulus of the matrix and the pulsed flux is small enough, far from the volume resonance of the shell, not to modify  $E_{\text{eff}}$  (see also Fig. 8 and the related discussion).

For shells having a hole, the system is given by Eq. (8) with the flux  $J = S_s u_s + S_n u_n$ . The acoustic absorption shown in Fig. 6b compares the experimental data to our model and to the low frequency approximation of the scattering model of Norris et al. (Eq. (67) in Ref. 13). The latter assumes that each elastic resonator behaves as in a free field. Note that the length of the Helmholtz resonator neck,  $l_n$ , was added to Norris original work established initially for holes through a shell with no thickness.

Both models are in fairly good agreement and describe the quarter wavelength ( $f_{\lambda/4} = 2100$  Hz) and the Helmholtz ( $f_H = 3150$  Hz) absorption frequencies well, although they differ slightly at higher frequencies. Our model predicts the  $3\lambda/4$  ( $f_{3\lambda/4} = 4600$  Hz) absorption quite accurately, where Norris' model overestimates the frequency of this peak absorption; this peak is however very sensitive to the parameters of the model. For both models, the prediction of the absorption magnitude is not as good as the location of the frequency peaks. This can be explained by leaks in the acrylic coating. A detailed discussion concerning the effect of the microporosity is provided in the next section.

In comparison, absorption is higher over the whole frequency range with soft shell resonators (fig. 6b) than with rigid counterparts (fig. 4b).

We can also observe a shift toward low frequencies of the Helmholtz absorption due to the elasticity of the shells as mentioned by Norris<sup>13</sup>. From Eq. (1), the shells used in this work lead to  $R_0 = 0.7$ . The error on the predicted Helmholtz frequency for the elastic shell ( $f_H = 3150$  Hz), with respect to the resonance frequency of rigid shells ( $f_H \approx 3500$  Hz), is below 10%.

### C. Elastic porous shells

Here, we consider microporous shells. The SEM photograph of the surface of a shell presented in Fig. 5b, shows that all the micropores have complex and different shapes. Considering a single geometry for all the

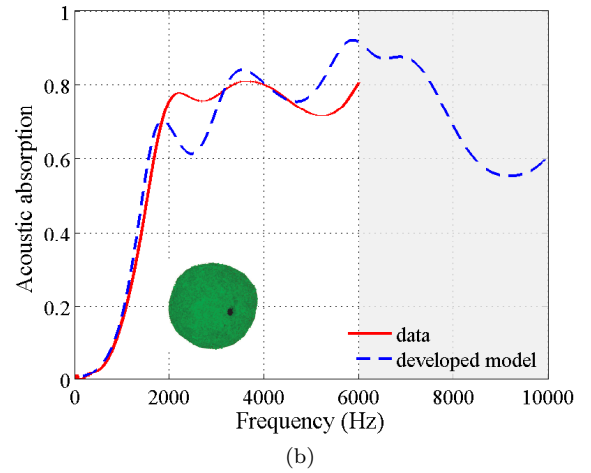
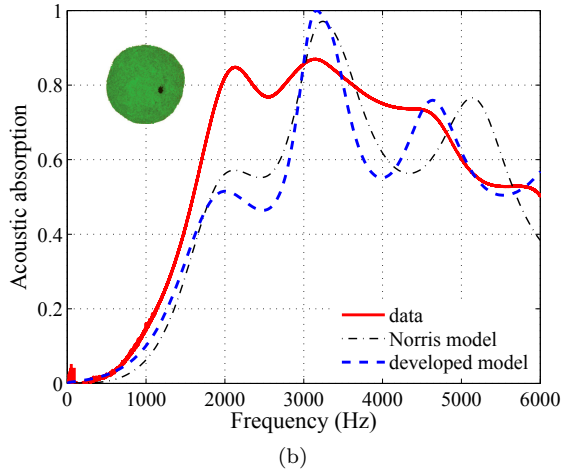
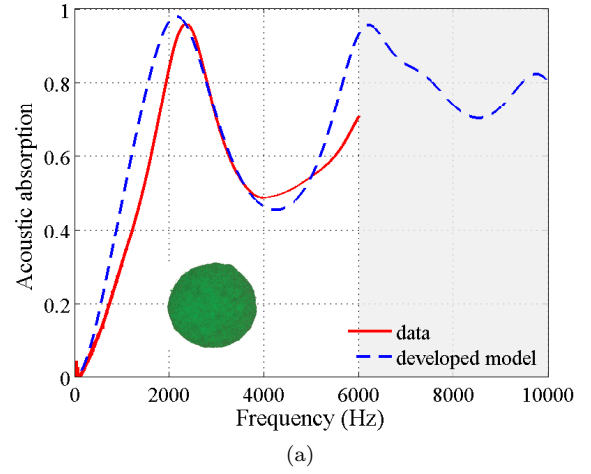
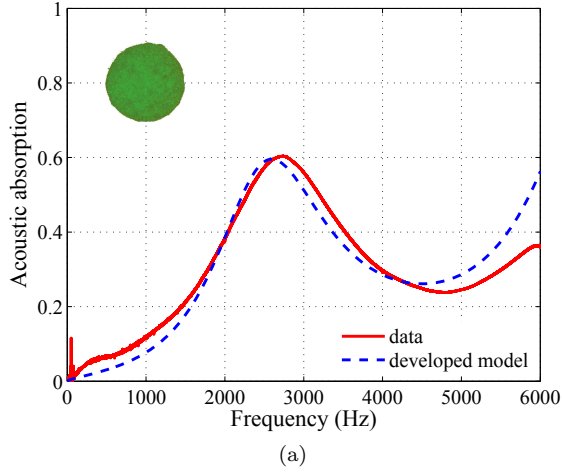


FIG. 6. Acoustic absorption measured for impervious elastomer shells (—) compared to the model developed (---) and the model adapted from Norris (- · -) for (a) non-drilled shells, (b) shells drilled with a 0.6 mm diameter hole.

micropores would lead to a poor description, by concentrating the absorption into a narrow frequency band. In the first approximation, we consider a uniform distribution of micropore radii, centered on the averaged radius ( $R_\mu = 33 \cdot 10^{-6}$  m) and a total microporosity equal to  $\phi_\mu = 1.82 \cdot 10^{-3}$ . Parameters  $R_\mu$  and  $\phi_\mu$  are both determined with the model fitted to measurements of acoustic absorption of non-drilled porous shells. Here, we consider  $N = \phi_\mu S_s / S_\mu$  holes with  $k$  different radii (between  $R_{\mu_1} = 20 \cdot 10^{-6}$  m and  $R_{\mu_2} = 50 \cdot 10^{-6}$  m). Each set of holes has the same weight  $\phi_\mu / k$ . The mean displacement of the air in the micropores is  $u_\mu^i$  (with  $i = 1, \dots, k$ ) and the associated viscous losses are taken into account. The equations of motion are thus

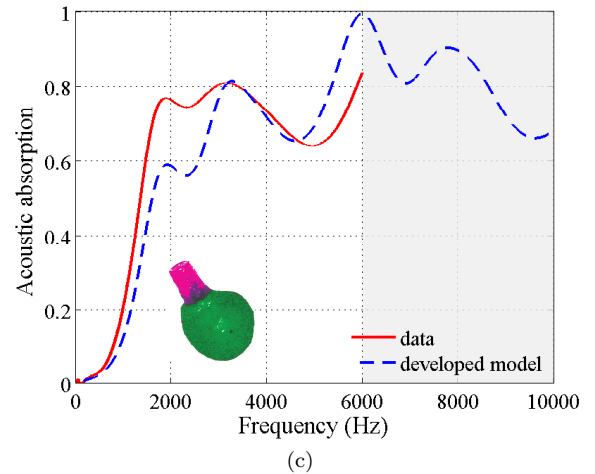


FIG. 7. Acoustic absorption measured for porous elastomer shells (—) compared to the model developed (---) for (a) non drilled shells, (b) shells drilled with a 0.6 mm in diameter hole, and (c) shells having a 1.3 mm in diameter and 5 mm long neck.

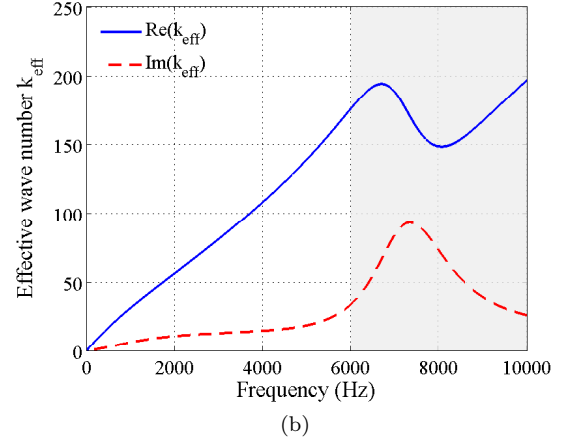
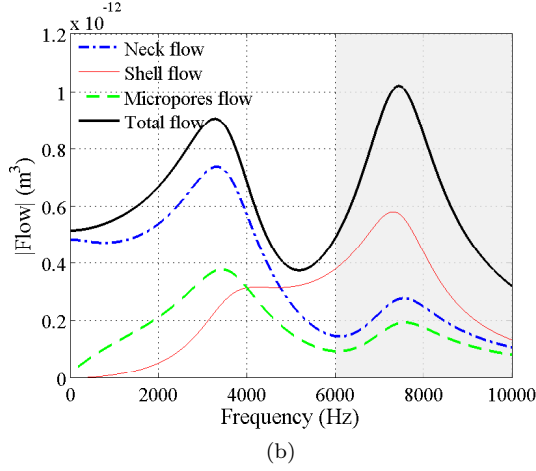
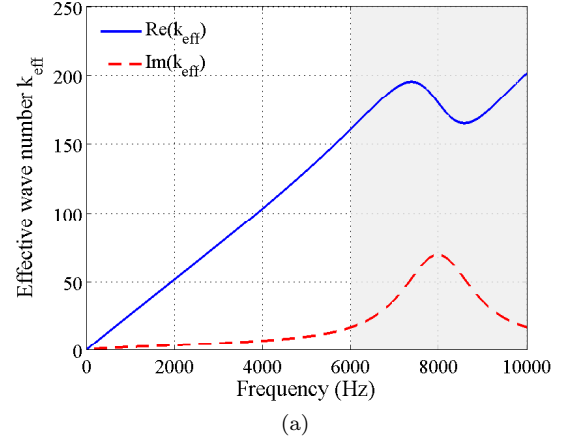
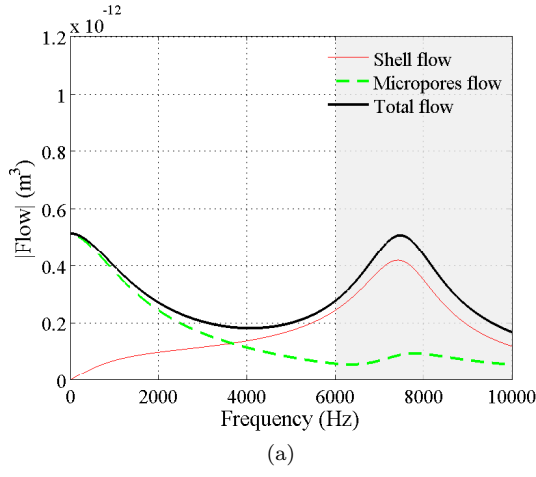


FIG. 8. Modulus of the outgoing fluxes to (a) non drilled shells and (b) shells with a 0.6 mm diameter neck. The curves correspond to the flux of the neck (-.-), of the shell (—), of the micropores (- -) and the total flux (—).

$$\left\{ \begin{array}{l} -\omega^2 m_n u_n = -S_n \frac{K_0}{V_0} J - p^{\text{ext}} S_n + F_n(u_n, u_s), \\ -\omega^2 m_s u_s = -k_s u_s - S_s \frac{K_0}{V_0} J - p^{\text{ext}} S_s - F_n(u_n, u_s) \\ \quad - N F_\mu(u_\mu, u_s), \\ -\omega^2 N' m_\mu u_\mu^1 = -N' S_\mu^1 \frac{K_0}{V_0} J - N' p^{\text{ext}} S_\mu^1 + N' F_\mu^1(u_\mu^1, u_s), \\ \quad \vdots \\ -\omega^2 N' m_\mu u_\mu^k = -N' S_\mu^k \frac{K_0}{V_0} J - N' p^{\text{ext}} S_\mu^k + N' F_\mu^k(u_\mu^k, u_s), \end{array} \right. \quad (15)$$

with  $N' = N/k$  and the flux  $J = (S_n u_n + S_s u_s + \sum_{c=1}^k N' S_\mu^c u_\mu^c)$ .

Absorption measurements are performed for the three cases presented in Fig. 3b whose corresponding heights and compactions are given in table III.

Figure 7 presents the experimental results obtained for each case together with the absorption calculated by our model. In the first case (Fig. 7a), when the granular

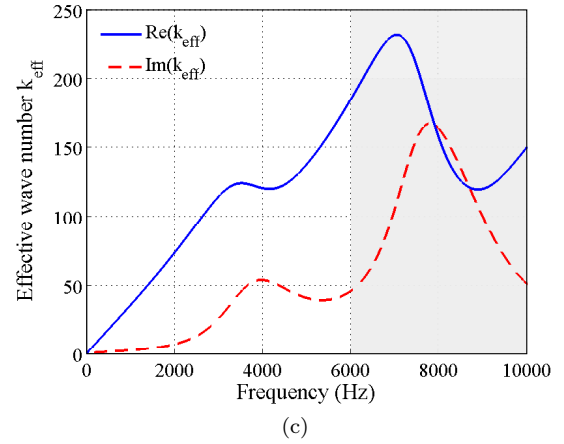


FIG. 9. Real part (—) and imaginary part (- -) of the effective wave number  $k_{\text{eff}}$  for (a) elastic, (b) non drilled porous shells and (c) porous shells with a 0.6 mm diameter neck.

medium is composed of non-drilled shells, the microporosity yields an absorption close to one at the quarter wavelength frequency although the quarter wavelength frequency is almost the same as for impervious shells. In addition, the slope of the acoustic absorption at low frequencies is steeper when the shell is microporous. This

Configurations	Height $h$	$C$
Undrilled	$25.86 \pm 1.13$ mm	0.56
Drilled ( $d_n = 0.6$ mm, $l_n = t$ mm)	$25.04 \pm 0.45$ mm	0.58
Neck ( $d_n = 1.3$ mm, $l_n = 5$ mm)	$28.56 \pm 1.99$ mm	0.51

TABLE III. Heights and capacities corresponding to the 60 porous shells.

is a typical result for a double porosity medium<sup>21,22</sup>. The inter-scale ratio between the mesopore radius  $r_p$  (air gap between the shells), and the micropore radius  $r_\mu$ ,  $\varepsilon_0 = r_\mu/r_p = 49.8 \cdot 10^{-3}$ , is small enough to be in line with the high-permeability contrast where the effects are strongest.

The model captures the acoustic behavior of the medium and predicts the quarter wavelength frequency ( $f_{\lambda/4} = 2360$  Hz) quite well despite the fact that the agreement may be artificial because of the fit.

Similarly, the measurements and the model are in good agreement when the pack is composed of porous Helmholtz resonators, with a neck (Fig. 7c) and without a neck (Fig. 7b). The quarter wavelength and the Helmholtz absorptions are well-predicted and the amplitudes are rendered faithfully.

Thus the model can also be used to evaluate the competition between the different fluxes. They are plotted up to 10 kHz, although the homogenization approach is not assumed as fully valid up to the upper bound frequency ( $\lambda/d_s \sim 5$  at 10 kHz) and coupling between resonators<sup>14</sup> may exist. It is nonetheless instructive to consider the theoretical absorptions and the corresponding fluxes. The fluxes are presented in Fig. 8 for the porous samples tested. As already observed by Norris *et al.*<sup>13</sup>, all the fluxes may have the same order of magnitude depending on the parameters chosen. As shown in Fig. 8a, without a hole the total flux is driven by the flow in the micropores up to 4000 Hz, leading to increased absorption at low frequencies. This characteristic is no longer visible when a hole is drilled in the shells. The flow through the neck overwhelms the flow through the micropores (as seen on figures 8b) and the increase of the absorption slope in the low frequency domain is no longer visible. As seen in figures 8b, the Helmholtz absorption frequency corresponds to a maximum of the flow originating from the neck, but the model also reveals the strong couplings between the shell and micropores close to this frequency.

At higher frequencies, the flow is clearly dominated by the shell breathing mode around 7500 Hz. In vacuo, this mode occurs<sup>16</sup> at 5800 Hz. Taking into account the air inside the shell, the frequency is shifted to 7400 Hz in our sample. The flux due to the shell can be considerable and complementary to the flux in the neck. For practical applications, softer shells can be used to shift the breathing mode down toward lower frequencies.

It can be seen in Fig. 9 that the Helmholtz resonance and shell breathing mode have similar effects on the effective wavenumber. They lead to a frequency band where the phase and the group velocities are opposite and to

strong attenuation (imaginary part of the wavenumber). This is a direct consequence of the effective bulk modulus  $E_{\text{eff}}$  since density  $\rho_{\text{eff}}$  is a regular function of the frequency. In order to maximize the attenuation close to the resonance, it is better to have a resonator with a high quality factor. It is noteworthy that without losses, the Helmholtz resonance leads to a band gap, i.e. to an imaginary wavenumber. As the damping tends to smooth the abrupt variations of the effective wavenumber (or of  $E_{\text{eff}}(\omega)$ ), losses in the resonator have to be small enough to maintain a strong imaginary part of the effective wavenumber (see Ref. 7 for detailed discussion on the parameter influencing the band gap). Furthermore, the dynamics in the micropores is dominated by the viscous force. This yields non-resonant over-damped oscillations (the damping ratio in the sample is high,  $\zeta \sim 2$  over the whole probed frequency range) that mainly modify the attenuation. Nonetheless, maximizing attenuation is useful but not sufficient to obtain good absorption since the latter results in a combination between attenuation and reflections at the interfaces with the air and with the rigid wall.

#### IV. CONCLUSIONS

In this work, we studied the acoustic absorption of granular media composed of shells made of different types of material (rigid, elastic and elastic and microporous) coupled or not with an Helmholtz resonator (drilled, extended neck).

For each case, the comparison between the acoustic absorption measurements and the models proposed showed that the main trends of acoustic behavior were well predicted. Nevertheless, capturing dissipation precisely was harder than identifying the absorption peak frequencies. For the elastic porous shell, one method of improvement was to measure  $R_\mu$  and  $\phi_\mu$  directly with a porosity-meter combined with a resistivity-meter and also measure the shell elasticity constant directly.

Each feature created a mass flux in the host medium that affected sound propagation. The different configurations measured and the model were used to analyze the contribution of each flux mechanism. It was shown that:

i) Helmholtz resonators can boost sound absorption close to their resonance frequency and lower the global effective bulk modulus<sup>7,8</sup>.

ii) The micropores can efficiently enhance absorption at low frequency when there is no neck. When a neck is present, they add broadband dissipation.

iii) Without a hole, the first breathing mode of the shell can be an efficient resonator. However, with the samples tested, this effect was mainly visible only in the simulations. When a neck was present, shell elasticity lowered the Helmholtz frequency. This shift was consistent with Eq. (1).

Optimizing the absorption of the materials required balancing the fluxes of the neck, shell and micropores. To do this, the critical coupling approach already applied to absorb sound with the Helmholtz resonator and membranes<sup>23</sup> appeared to be a promising design option.

Another path of enhancement is to mix different grain sizes to fill the interstices and increase viscothermal losses in the host medium.

Porogranular material are promising and can absorb sound waves more efficiently than rigid grains. Since each grain is an *independent* and *customizable* building block, this method provides a very versatile class of acoustic metamaterials. The encouraging results obtained in this work lead us to consider extending this study to transmission insulation using thinner and softer resonators. This may make it possible for us to observe nonlinear wave propagation through hollow spherical shells, as shown in Ref. 24.

### Acknowledgment

Support for this work was received from the French Research National Agency and the Research Foundation for Aeronautics and Space (ANR METAUDIBLE No. ANR-13-BS09-0003).

### APPENDIX A: RIGID FRAME MODEL

The effective modulus of the porous matrix  $E_m(\omega)$  and the effective density  $\rho_{\text{eff}}(\omega) = \rho_m(\omega)$  are calculated using the Johnson-Champoux-Allard equivalent fluid model. They take into account thermal and viscous losses and are defined by :

$$E_m(\omega) = \gamma P_0 \left[ \gamma - (\gamma - 1) \left( 1 - \frac{j\omega_\nu \tilde{G}(\omega Pr)}{\omega Pr} \right)^{-1} \right]^{-1}, \quad (\text{A1})$$

$$\rho_m(\omega) = \frac{\rho_0 \alpha_\infty}{\phi} \left( 1 - \frac{j\omega_\nu \tilde{F}(\omega)}{\omega} \right), \quad (\text{A2})$$

where  $\omega_\nu = \sigma\phi/\rho_0\alpha_\infty$  is the viscous frequency,  $\gamma$  is the specific heat ratio,  $P_0$  is the atmospheric pressure,  $Pr$  is the Prandtl number,  $\rho_0$  is the density of the fluid in the pores,  $\phi$  is the porosity,  $\alpha_\infty$  is the tortuosity, and  $\sigma$  is the flow resistivity. The correction functions  $\tilde{G}(\omega Pr)$ <sup>25</sup> and  $\tilde{F}(\omega)$ <sup>26</sup> are given by :

$$\begin{aligned} \tilde{G}(\omega Pr) &= \left[ 1 - j\eta\rho_0 Pr \omega \left( \frac{2\alpha_\infty}{\sigma\phi\Lambda'} \right)^2 \right]^{1/2}, \\ \tilde{F}(\omega) &= \left[ 1 - j\eta\rho_0 \omega \left( \frac{2\alpha_\infty}{\sigma\phi\Lambda} \right)^2 \right]^{1/2}, \end{aligned} \quad (\text{A3})$$

where the terms  $\Lambda$  and  $\Lambda'$  are the viscous and thermal characteristic lengths respectively and  $\eta$  is the dynamic viscosity of the fluid. According to the sphere diameters, here we use the following parameters given by Allard<sup>1</sup>. These parameters have also been used in Refs.<sup>3,6</sup>. The resistivity of the matrix is  $\sigma = 4\eta F/\Lambda^2$  with the formation factor  $F = 3.4$ . The thermal characteristic length is given by  $\Lambda' = \phi d_s/3(1 - \phi)$  and the viscous characteristic length is estimated as  $\Lambda = \Lambda'/3$ . The only exception

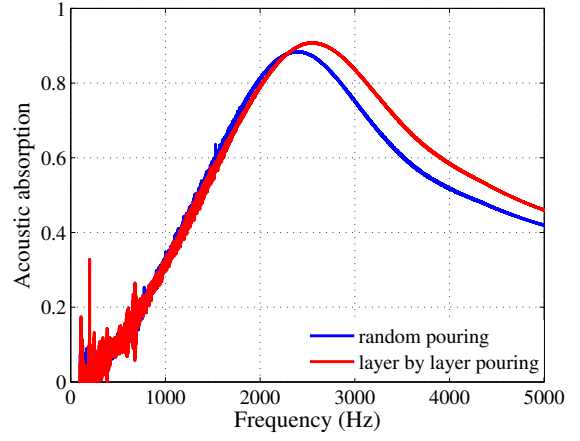


FIG. 10. Acoustic absorption obtained for different pouring methods.

with Allard<sup>1</sup> is the high frequency limit of tortuosity, which we set at  $\alpha_\infty = 1.5$ , instead of 1.36. Boutin et al.<sup>2</sup> indeed showed that  $\alpha_\infty$  strongly depends on the compaction close to  $\phi \approx 0.5$ . As an example, for  $C = 0.53$ , the different parameters take the values  $\sigma = 760 \text{ N.s.m}^{-4}$ ,  $\Lambda = 552 \mu\text{m}$  and  $\Lambda' = 1700 \mu\text{m}$ .

### APPENDIX B: ARRANGEMENT OF THE GRANULAR PACKING

Different measurements with the same number of porous grains were performed for various pouring methods: the grains were poured randomly (compaction: 0.61, height: 25.5 mm) or layer by layer (compaction: 0.63, height: 22.5 mm). The experimental results are presented in Fig.10. Regarding the same number of grains, low compaction packing is higher. Maximum absorption occurs at lower frequency for low compaction than for high compaction packing.

- <sup>1</sup> J. F. Allard, M. Henry, J. Tizianel, L. Kelder, and W. Lauriks, "Sound propagation in air-saturated random packings of beads", J. Acoust. Soc. Am. **104**, 2004–2007 (1998).
- <sup>2</sup> C. Boutin and C. Geindreau, "Periodic homogenization and consistent estimates of transport parameters through sphere and polyhedron packings in the whole porosity range", Phys. Rev. E **82**, 036313 (2010).
- <sup>3</sup> O. Dazel and V. Tournat, "Nonlinear biot waves in porous media with application to unconsolidated granular media", J. Acoust. Soc. Am. **127**, 692–702 (2009).
- <sup>4</sup> J.-D. Chazot and J.-L. Guyader, "Transmission loss of double panels filled with porogranular materials", J. Acoust. Soc. Am. **126**, 3040–3048 (2009).
- <sup>5</sup> J.-D. Chazot and J.-L. Guyader, "Acoustic modeling of light and non-cohesive poro-granular materials with a fluid/fluid model", Acta Mech. **195**, 227–247 (2008).
- <sup>6</sup> B. Nennig, Y. Renou, J.-P. Groby, and Y. Aurégan, "A mode matching approach for modeling two dimensional porous grating with infinitely rigid or soft inclusions", J. Acoust. Soc. Am. **131**, 3841–3852 (2012).

- <sup>7</sup> C. Boutin, “Acoustics of porous media with inner resonators”, *J. Acoust. Soc. Am.* **134**, 4717–4729 (2013).
- <sup>8</sup> C. Boutin and F.-X. Becot, “Theory and experiments on poro-acoustics with inner resonators”, *Wave Motion* **54**, 76–99 (2015).
- <sup>9</sup> J.-P. Groby, B. Nennig, C. Lagarrigue, B. Brouard, O. Dazel, and V. Tournat, “Enhancing the absorption properties of acoustic porous plates by periodically embedding helmholtz resonators”, *J. Acoust. Soc. Am.* **137**, 273–280 (2015).
- <sup>10</sup> N. Fang, D. Xi, J. Xu, M. Ambati, W. Srituravanich, C. Sun, and X. Zhang, “Ultrasonic metamaterials with negative modulus”, *Nat. Mater.* **5**, 452–456 (2006).
- <sup>11</sup> T. Weisser, J.-P. Groby, O. Dazel, F. Gaultier, E. Deckers, S. Futatsugi, and L. Monteiro, “Acoustic behavior of a rigidly backed poroelastic layer with periodic resonant inclusions by a multiple scattering approach”, *J. Acoust. Soc. Am.* **139**, 617–629 (2016).
- <sup>12</sup> D. M. Photiadis, “The effect of wall elasticity on the properties of a Helmholtz resonator”, *J. Acoust. Soc. Am.* **90**, 1188–1190 (1991).
- <sup>13</sup> A. N. Norris and G. Wickham, “Elastic Helmholtz resonators”, *J. Acoust. Soc. Am.* **93**, 617–630 (1993).
- <sup>14</sup> C. Lagarrigue, J.-P. Groby, V. Tournat, O. Dazel, and O. Umnova, “Absorption of sound by porous layers with embedded periodic array of resonant inclusions”, *J. Acoust. Soc. Am.* **134**, 4670–4680 (2013).
- <sup>15</sup> K. U. Ingard, “On the theory and design of acoustic resonators”, *J. Acoust. Soc. Am.* **25**, 1073 (1953).
- <sup>16</sup> W. E. Baker, “Axisymmetric modes of vibration of thin spherical shell”, *J. Acoust. Soc. Am.* **33**, 1749 (1961).
- <sup>17</sup> J.-F. Allard and N. Atalla, *Propagation of Sound in Porous Media: Modeling Sound Absorbing Materials (second edition)*, 372pp (John Wiley & Sons, Chichester) (2009).
- <sup>18</sup> J.-C. Le Roux, M. Pachebat, and J.-P. Dalmont, “A new impedance sensor for industrial applications”, in *Acoustics 2012*, edited by S. F. d’Acoustique (Nantes, France) (2012).
- <sup>19</sup> C. Zwikker and C. Kosten, *Sound absorbing materials.*, 180pp (Elsevier, New York) (1949).
- <sup>20</sup> H. A. Makse, N. Gland, D. L. Johnson, and S. L., “Granular packings: Nonlinear elasticity, sound propagation, and collective relaxation dynamics”, *Phys. Rev. E* **70**, 061302 (2004).
- <sup>21</sup> X. Olny and C. Boutin, “Acoustic wave propagation in double porosity media”, *J. Acoust. Soc. Am.* **114**, 73–89 (2003).
- <sup>22</sup> R. Venegas and O. Umnova, “Acoustical properties of double porosity granular materials”, *J. Acoust. Soc. Am.* **130**, 2765–2776 (2011).
- <sup>23</sup> V. Romero-Garcia, G. Theocharis, O. Richoux, A. Merkel, V. Tournat, and V. Pagneux, “Perfect and broadband acoustic absorption by critically coupled sub-wavelength resonators”, *Sci. Rep.* **6**, 19519 (2016).
- <sup>24</sup> D. Ngo, S. Griffiths, D. Khatri, and C. Daraio, “Highly nonlinear solitary waves in chains of hollow spherical particles”, *Granul. Matter* **15**, 149–155 (2013).
- <sup>25</sup> J.-F. Allard and Y. Champoux, “New empirical equations for sound propagation in rigid frame porous materials”, *J. Acoust. Soc. Am.* **91**, 3346–3353 (1992).
- <sup>26</sup> D. L. Johnson, J. Koplik, and R. Dashen, “Theory of dynamic permeability and tortuosity in fluid-saturated porous media”, *J. Fluid. Mech.* **176**, 379–402 (1987).